Research Article | Vol. 27, No. 21 / 14 October 2019 / Optics Express 29685
Optics EXPRESS

Optical singularities and Möbius strip arrays in tailored non-paraxial light fields

KEMAL TEKCE, EILEEN OTTE,* AND CORNELIA DENZ

Institute of Applied Physics, University of Muenster, Corrensstr. 2/4, 48149 Muenster, Germany
*eileen.otte@uni-muenster.de

Abstract: A major current challenge in the field of structured light represents the development from three- (3d) to four-dimensional (4d) electric field structures, in which one exploits the transverse as well as longitudinal field components in 3d space. For this purpose, non-paraxial fields are required in order to be able to access visionary 3d topological structures as optical cones, ribbons and Möbius strips formed by 3d polarization states. We numerically demonstrate the customization of such complex topological structures by controlling generic polarization singularities in non-paraxial light fields. Our approach is based on tightly focusing tailored higher-order vector beams in combination with phase vortices. Besides demonstrating the appearance of cones and ribbons around the optical axis, we evince sculpting arrays of Möbius strips realized around off-axis generic singularities.

1. Introduction

Structured light has achieved paramount importance within the last decades [1–4]. On the one hand, structured light fields enable advanced applications in areas such as optical manipulation [5–7], classical as well as quantum information technologies [8–11], material machining [12,13], metrology [14,15], and high-resolution imaging [16,17]. On the other hand, light fields structured in its different degrees of freedom have proven to be fundamentally meaningful, unveiling elementary properties of electromagnetic waves especially with respect to optical singularities (e.g. [2,3]). These fields are not only artificially created by different means of sculpting light as by spatial light modulators (SLMs) [18–23], q-plates [24], interferometric techniques [21,25–28], and many more, but also appear in nature in the blue daylight sky or in optical speckle fields [3,29]. Hence, the study of complex singular light fields enables new insights into the general and not yet fully explored, nor understood, nature of light.

Recently, in addition to spatially structuring the amplitude and phase of light, spatially shaping the polarization as a third degree of freedom has come to the fore, mainly enabled by advances in modulation techniques [1,19,23–25,30]. Even though the importance of polarization modulation has quickly been accepted, current findings are mainly limited to the paraxial regime. Consequently, investigations were concentrated on three-dimensional (3d) fields $\mathbf{E}(x, y, z)$ of two-dimensional (2d) polarization, in which the polarization of light is purely transverse, oscillating solely within the plane orthogonal to the beam's propagation direction. However, polarization of light is a three-dimensional feature, including full elliptical polarization states. A major current challenge is therefore the development from these spatial 3d structures of 2d polarization to four-dimensional (4d) cases, exploiting all three field components $\boldsymbol{\mathcal{E}}(x, y, z) = [\mathcal{E}_x(x, y, z), \mathcal{E}_y(x, y, z), \mathcal{E}_z(x, y, z)]^T$, i.e. the longitudinal in addition to typical transverse electric field contributions. Similar to 4d materials, the term 4d light fields is chosen for fields which are structured in 3d space and additionally include a fourth dimension [31]. This dimension can be accessed in non-paraxial light fields as e.g. in tightly focused beams where radial components of the input light field form significant longitudinal focal field contributions [32–35] as the focal

#370385 https://doi.org/10.1364/OE.27.029685
Journal © 2019 Received 19 Jun 2019; revised 7 Aug 2019; accepted 7 Aug 2019; published 1 Oct 2019

Optics EXPRESS

field's fourth dimension [31]. However, strong focusing brings theoretical investigations out of the paraxial regime, and thus represents a major actual conceptional challenge. Consequently, only few studies up to now represent the spearhead towards the understanding of 4d field structures and its subsequent implementation, applying tight focusing properties of polarization structures e.g. for the creation of tailored focal fields [34,36–39] as optical needles. From a fundamental perspective, longitudinal field components enable the formation of complex 3d polarization topologies as optical cones, twisted ribbons and Möbius strips, as first predicted by I. Freund [40] and experimentally proven by T. Bauer et al. in 2015 [41,42]. Typically, these topologies appear around generic polarization singularities, namely, C-points (points of pure circular polarization) and L-points (points of pure linear polarization), in which the orientation or handedness of polarization is undefined, respectively [43–47]. Within the 3d volume of a non-paraxial 4d field, these singularities form lines of pure circular or linear polarization meandering throughout 3d space, appearing as points if a chosen 2d plane is considered. The investigation of the 3d polarization ellipses around these singular points can reveal complex topologies forming intended cones, ribbons or Möbius strips.

First simple but yet striking examples of 3d polarization topologies have been demonstrated recently [41,42,48–52], not only by tight focusing but also off-axis interference of two customized beams [48], scattering from high-index dielectric nano-particles [50], or by the application of all-dielectric metasurfaces [52]. However, a general framework to access intriguing 4d structures of light revealing sophisticated even not yet known topologies has not yet been developed. Within our study, we numerically evince the on-demand customization of generic polarization singularities in 3d space and, thus, of complex optical topologies in the non-paraxial regime. We are even able to demonstrate the formation of a customizable polarization Möbius strip array. Our method is based on defined tailoring of non-paraxial light fields by tightly focusing vector beams of spatially varying linear polarization in combination with additional phase vortices (see Sec. 2.). We apply vector fields of higher order [35,53], i.e. the states of polarization surrounding the included non-generic V-point singularity of undefined polarization [3,35] rotate multiple times while going around the on-axis singularity. By the inclusion of an additional phase vortex embedding a point of undefined phase (phase singularity), we change the symmetry of the vector beam in such a way that the resulting focal 4d light field includes unknown 3d topologies centered on- (see Sec. 3.) as well as off-axis (see Sec. 5.) within the focal 2d plane ($z = 0$). We demonstrate the control of C- and L-singularities (see Sec. 4.) in the non-paraxial regime by adapting the phase and polarization singularity indices σ_{12} and l, respectively, of the incident paraxial light field, proving the ability to customize intriguing topological structures even at the nanoscale of strongly focused light.

2. Method

In general, paraxial vector fields exhibit an inhomogeneous polarization distribution in which the polarization in the transverse plane covers only the equator of the Poincaré sphere, thus containing exclusively linear states of polarization [35,47,54–56]. In such paraxial fields the inhomogeneous distribution of linear polarization states can result in non-generic vectorial polarization singularities, namely V-points, in which the complex electric field vector $\mathbf{E} = [E_x, E_y]^T$ ($E_z \approx 0$) and therefore the polarization cannot be defined [57,58]. In order to describe the singularity and the transverse pattern of different vector fields, the complex Stokes field

$$\Sigma_{12} = S_1 + \mathrm{i}S_2 = A_{12} \exp(\mathrm{i}\phi_{12}) \tag{1}$$

with $A_{12} = \sqrt{S_1^2 + S_2^2}$ and $\phi_{12} = \arg(\Sigma_{12})$ is defined for the paraxial regime [57–59]. Here, S_i with $i = \{0, 1, 2, 3\}$ represent the normalized Stokes parameters. Thus, V-points can be identified as phase singularities in ϕ_{12}, and are characterized by the Stokes field index $\sigma_{12} = \frac{1}{2\pi} \oint \mathrm{d}\phi_{12}$ [57,59]

Optics EXPRESS

($|\sigma_{12}|/2 \in \mathbb{N}$; $\sigma_{12} = 2\eta$, η: Poincaré-Hopf index [57]) representing its order. Furthermore, a relation between singularity index and overall polarization distribution can be found [53,58]. Examples for vector fields including singularities are illustrated in Fig. 1. Here, the polarization distribution as well as the phase ϕ_{12} of two different higher-order vector beams with $\sigma_{12} = \pm 8$ are presented. Solid black lines depict linear polarization states and solid red lines visualize the flow lines. Around V-points with a positive singularity index ($\sigma_{12}>2$), a flower-like polarization distribution is found, whereas for a negative singularity index ($\sigma_{12}<-2$), a spider-web-like structure appears. These higher-order structures typically contain $|\sigma_{12} - 2|$ ζ-lines, along which the polarization states are oriented radially towards the on-axis singularity [47], and $|\sigma_{12} - 2|$ flower petals or spider web sectors, respectively. Hence, the number of radial components inside transverse patterns of a vector beam is strongly related to the V-point and its singularity index. This feature of vector beams is key for controlling singularities as well as complex topologies in tightly focused light fields, as we will prove in the following sections.

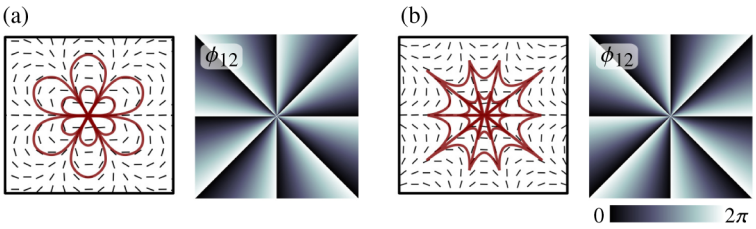

Fig. 1. Higher-order vector beams with singularity index (a) $\sigma_{12} = 8$ and (b) $\sigma_{12} = -8$ forming vectorial flowers and spider webs, respectively. Illustrated are the linear polarization distributions including red flow lines and the corresponding Stokes field phase ϕ_{12}.

We investigate the tightly focusing properties of flower- and web-shaped vector fields of index σ_{12} including additional global phase vortices of topological charge l (counterclockwise azimuthal change of phase around on-axis phase singularity divided by 2π). These paraxial vectorial fields can be described by

$$\mathbf{E}_{\text{in}} = \left[\cos\left(\frac{\sigma_{12}}{2}\cdot\varphi\right), \sin\left(\frac{\sigma_{12}}{2}\cdot\varphi\right)\right]^T \cdot \exp\left(\mathrm{i}l\varphi\right) \tag{2}$$

with $|\sigma_{12}|/2 \in \mathbb{N}$ and the azimuthal angle $\varphi \in [0, 2\pi]$ in polar coordinates. Note that *global* phase vortices do not effect the polarization structure at $z = 0$. This means, in the presented case, the paraxial polarization distribution for $l = 0$ and $l \neq 0$ is the same, representing flower or web structures, purely defined by the σ_{12} dependent vector in Eq. (2).

In general, by tightly focusing a paraxial light field, e.g. vector beam, a non-negligible longitudinal polarization component is created and the complex electric field vector $\boldsymbol{\mathcal{E}} = [\mathcal{E}_x, \mathcal{E}_y, \mathcal{E}_z]^T$ is no longer purely transverse with $\mathcal{E}_z \approx 0$, but three-dimensionally oriented with $\mathcal{E}_z \neq 0$ [33,60,61]. In order to determine the focal electric field $\boldsymbol{\mathcal{E}}$ and its components $\mathcal{E}_x, \mathcal{E}_y$, and $\mathcal{E}_z$ with $\mathbf{E}_{\text{in}}$ as input light field, we solve Richards and Wolf integrals [60] by using a fast Fourier transform operation as described in [34,62]. Numerically calculating the focal field distribution $\boldsymbol{\mathcal{E}}$ (numerical aperture NA = 0.9, refractive index $n = 1$), we examine the resulting polarization pattern inside the tight focus ($z = 0$) with respect to its non-paraxial 3d polarization singularities and its hidden topological structures.

3. From cone to strip

By tightly focusing higher-order vector beams, an inhomogeneous 2d polarization pattern of linear states is transformed into a complex arrangement of elliptical 3d polarization states in 3d space [40–42,63–66]. Consequently, 4d fields are formed. In order to determine the polarization

Optics EXPRESS

distribution in such a non-paraxial field, we only consider polarization states inside the focal plane, i.e. $z = 0$. We use the calculated electric field vector $\boldsymbol{\mathcal{E}}(\mathbf{r}) = [\mathcal{E}_x(\mathbf{r}), \mathcal{E}_y(\mathbf{r}), \mathcal{E}_z(\mathbf{r})]^T$ with $\mathbf{r} = (x, y, z)^T$ to trace the polarization ellipses and their respective 3d orientation in this plane.

In contrast to paraxial light fields, conventional Stokes parameter analysis cannot be applied to understand the polarization distribution in non-paraxial light fields and therefore in the focal plane due to the 3d electric field nature in each plane. In the non-paraxial regime, Stokes parameters would require an extension to 3d to be applicable [67,68]. However, the full structure can be deciphered by deriving the major axis $\boldsymbol{\alpha}$, minor axis $\boldsymbol{\beta}$ and normal vector $\boldsymbol{\gamma}$ of the polarization ellipse defined by [69]

$$\boldsymbol{\alpha} = \frac{1}{|\sqrt{\boldsymbol{\mathcal{E}}\boldsymbol{\mathcal{E}}}|}\Re\left(\boldsymbol{\mathcal{E}}\sqrt{\boldsymbol{\mathcal{E}}^*\boldsymbol{\mathcal{E}}^*}\right), \qquad \boldsymbol{\beta} = \frac{1}{|\sqrt{\boldsymbol{\mathcal{E}}\boldsymbol{\mathcal{E}}}|}\Im\left(\boldsymbol{\mathcal{E}}\sqrt{\boldsymbol{\mathcal{E}}^*\boldsymbol{\mathcal{E}}^*}\right), \qquad \boldsymbol{\gamma} = \Im\left(\boldsymbol{\mathcal{E}}^* \times \boldsymbol{\mathcal{E}}\right), \tag{3}$$

Tightly focusing pure vector beams (Eq. (2) with $l = 0$) result in a focal polarization distribution ($z = 0$) where all major axes either lie in the focal plane or are perpendicular to it. This effect is due to the discrete relative phase values observed for the transverse (0 or π) and longitudinal ($\pi/2$ or $3\pi/2$) component, in this case, only allowing for these orientations, as evident from our previous work [34]. In contrast, combining these vector beams with phase vortices, a variety of polarization topologies is expected due to symmetry breaking between orthogonally polarized contributions of $\mathbf{E}_{\text{in}}$: Typically, paraxial vector modes can be represented as superpositions of orthogonal spatial modes of likewise orthogonal polarization. For circular polarization bases, spatial modes carry opposite helical charges with $l_{1,2} = \pm\sigma_{12}/2$, whose relation will be distorted by the intended addition of phase vortices resulting in a change of focal topology. To analyze this effect by an illustrative example, we calculate the electric field distribution $\boldsymbol{\mathcal{E}}(x, y, 0)$ of a focused vectorial flower structure with $\sigma_{12} = 8$ and an additional phase vortex of topological charge $l = 1$. This phase vortex causes the intended asymmetry with the respective paraxial field carrying vortices of charge $\pm\sigma_{12}/2 + l$, i.e. $l_1 = 4 + 1 = 5$ and $l_2 = -4 + 1 = -3$, in its two circular polarization bases.

Numerical results are shown in Fig. 2, where 2(a) illustrates the normalized intensity contributions $|\mathcal{E}_{x,y,z}|^2 \in [0, 1]$ as well as the phase distributions $\varphi_{x,y,z} \in [0, 2\pi]$ of each electric field component, 2(b) the total intensity distribution $|\boldsymbol{\mathcal{E}}|^2 \in [0, 1]$ and 2(c)–2(e) the created polarization topologies in the focal plane ($z = 0$). The ratio between the maximum intensity of $|\mathcal{E}_{x,y,z}|^2$ to the maximum of $|\boldsymbol{\mathcal{E}}|^2$ is written in white letters within intensity illustrations. We determine the polarization topology on circles around the optical axis having three different radii, shown as dashed white lines in 2(a) and 2(b). We trace the major axis (blue lines with blue and green ending points in Figs. 2(c)–2(e)) of the polarization ellipses which are located on these circles with 2(c) corresponding to the smallest circle, 2(d) to the medium sized circle and 2(e) to the largest circle. In the xy-plane, the projections of the polarization topologies are visualized.

The focused vectorial flower configuration reveals an eight-lobe intensity structure for its transverse components and a six-lobe structure for its longitudinal component as well as in its total intensity distribution, as illustrated in Figs. 2(a) and 2(b). Similar intensity distributions are generated if we focus the vectorial flower structure without a phase vortex [31,34,70]. In this case, as outlined in [34], the number of focal intensity lobes is related to the singularity index σ_{12} or, more precisely, the number of ζ-lines of the input field given by $|\sigma_{12} - 2|$: Purely radially oriented states as found on ζ-lines create maxima in longitudinal components, thus, $|\mathcal{E}_z|^2$ includes $|\sigma_{12} - 2|$ maxima. Further, x- and y-oriented focal components reveal $|\sigma_{12}|$ maxima at positions corresponding to the input field's horizontal and vertical polarization components. Even though the intensity distributions for a focused vectorial flower without and with a phase vortex ($l = 1$) resemble, the key difference of both focal structures is hidden in the phase distribution of each component which change dramatically if the vortex is added, resulting in intriguing 3d polarization topologies.

Optics EXPRESS

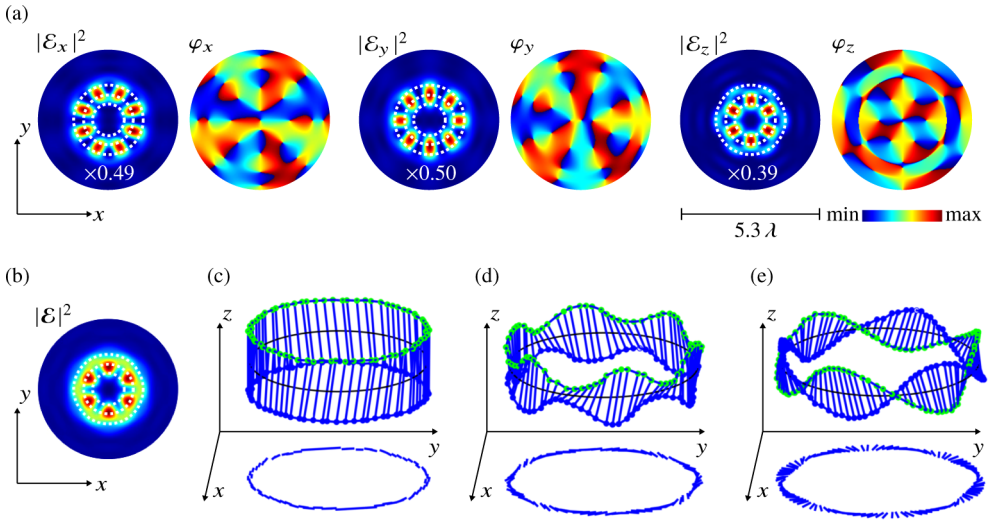

Fig. 2. Polarization topologies around the optical axis: We show the intensity distribution of (a) each component $|\mathcal{E}_{x,y,z}|^2 \in [0,1]$ and their respective phase $\varphi_{x,y,z} \in [0, 2\pi]$ as well as (b) the total intensity structure $|\mathcal{E}|^2 \in [0,1]$ of a tightly focused vector beam with the singularity index $\sigma_{12} = 8$ and a topological charge of $l = 1$ ($z = 0$). All intensity structures are normalized with respect to their maximum, whereby the ratio of the maximum of $|\mathcal{E}_{x,y,z}|^2$ to the one of $|\mathcal{E}|^2$ is shown within the intensity images in (a). Furthermore, (c)-(e) 3d polarization topologies inside the focal 2d plane are shown, whereby each topology is observed by tracing the major axis (blue lines with blue and green endpoints) on three different circles (white dashed line in (b) $|\mathcal{E}|^2$ and its components (a) $|\mathcal{E}_{x,y,z}|^2$; $z = 0$). The black circles in (c), (d), and (e) correspond to the small, medium, and large white circle in (b) at $z = 0$, respectively.

The created electric field and its phase distributions yield different topological structures for each circle. For the smallest circle, a cone-like structure is observed with respect to the major axis of the polarization ellipses (Fig. 2(c)). On this circle, a stronger longitudinal z-component than transverse x-/y-component can be found, causing the major axis to be arranged in a cone structure. By increasing the radius of the circle the transverse components become stronger. Therefore, the major axis starts to wiggle in the transverse directions as illustrated in Fig. 2(d). Hence, the cone structure degenerates into a ribbon topology without full twists on the medium sized circle. Here, the longitudinal component is still the dominant one, such that no twists are generated by the major axis. In contrast, by exploring the major axes on the largest circle 2(e), the focal field reveals a twisted ribbon topology with six twists, since the azimuthal periodicity of intensity lobes and phase values changed significantly for longitudinal components on this circle (cf. Fig. 2(a), $|\mathcal{E}_z|^2$). The number of twists corresponds to the number of maximal intensity lobes in $|\mathcal{E}_z|^2$ and to the number of ζ-lines in the incident vector beam, respectively.

In general, a fundamental relation can be observed between the twisted ribbon structure and the incident vector field with respect to the singularity index σ_{12} and the topological charge l. We explored the topological structures created inside the focal field for different singularity indices $\sigma_{12} \in [4, 10]$ and topological charges $l \in [0, 7]$ of the incident vector beam. For a chosen singularity index σ_{12} and a topological charge of $0 < l < |\sigma_{12}/2| - 1$, the focal field and its polarization topologies reveal a similar behavior like in Fig. 2. Consequently, the major axes create cone structures as well as twisted ribbons with $|\sigma_{12} - 2|$ twists for certain radii of the circles. As evident from our previous work in [31], larger topological charges ($l \leq |\sigma_{12}/2| - 1$)

Optics EXPRESS

result in a point or donut-like intensity structure, which yield cone topologies or ring structures, where all the major axis lie in the focal plane.

Hence, tightly focusing higher-order vector beams including phase vortices can form intriguing 3d topological structures with respect to their polarization ellipses around the optical axis. Furthermore, these topologies, e.g. the twisted ribbons, can be controlled by the focused singularity index σ_{12} and the topological charge l, allowing us to create arbitrary ribbons with a defined number of twists. In the following, we will explore on- as well as off-axis generic polarization singularities and their immediate surrounding topologies to obtain a deeper understanding of the generated polarization pattern inside these focused vector fields.

4. Controlling C- and L-singularities

Sophisticated 3d polarization topologies like Möbius strips are typically hidden around generic polarization singularities in non-paraxial 4d light fields [71,72]. These generic singularities, being stable upon minor perturbation [73], are meandering lines of circular and linear polarization in 3d space. If these lines pierce a 2d plane, e.g. the focal plane, points of pure circular polarization, C-points, and points of linear polarization, L-points, appear. Here, we search for and investigate these polarization singularities in tightly focused higher-order vector beams with additional phase vortices.

In the representation of Eq. (3) for the 3d polarization ellipse, a C-point arises if the polarization ellipse degenerates into a circle in which the major and minor axis cannot be specified, i.e. $\boldsymbol{\alpha} = \boldsymbol{\beta}$. Moreover, the 3d electric field vector $\boldsymbol{\mathcal{E}}$ and the rectifying phase θ define the complex scalar field [69]

$$\Psi_C = \boldsymbol{\mathcal{E}} \cdot \boldsymbol{\mathcal{E}} = (\boldsymbol{\alpha}^2 - \boldsymbol{\beta}^2) e^{\mathrm{i}2\theta} \tag{4}$$

which gives zero ($\Psi_C = 0$) if a C-point arises [65,69,74]. Thus, by calculating the intersection of the zero-lines $\Re(\Psi_C) = 0$ and $\Im(\Psi_C) = 0$ inside the focal plane of our focused vector beams, generic C-points can be located. In contrast, an L-point is created if the polarization ellipse degenerates into a line, thus the minor axis vanishes while the major axis remains well defined, leading to the normal vector $\boldsymbol{\gamma} = \mathbf{0}$ [69]. Consequently, the zero-lines corresponding to the components of the normal vector $\boldsymbol{\gamma} = (\gamma_x, \gamma_y, \gamma_z)$ can be used to find L-points in the focal plane.

For our analysis, we first numerically calculate the tight focus ($z = 0$) of a particular vector beam with an optional additional phase vortex. Second, we use the calculated focal electric field vector $\boldsymbol{\mathcal{E}}$ to determine the complex scalar field Ψ_C by Eq. (4) and the normal vector $\boldsymbol{\gamma}$ by Eq. (3). Furthermore, by means of the zero-lines of $\Re(\Psi_C)$, $\Im(\Psi_C)$ and $\gamma_{x,y,z}$, the generated focal polarization distribution can be searched for polarization singularities.

In Fig. 3 we illustrate the numerically calculated zero-lines of 1) $\Re(\Psi_C)$, $\Im(\Psi_C)$, and 2) $\gamma_{x,y,z}$ on the intensity distribution $|\boldsymbol{\mathcal{E}}|^2$ of tightly focused flower vector beams with $\sigma_{12} = 8$ and topological charge $l \in [0, 5]$. For the case of 3(a) $\sigma_{12} = 8$ and $l = 0$, the zero-lines 3(a1) $\Re(\Psi_C)$ (blue) and $\Im(\Psi_C)$ (orange) lie on top of each other, thus, instead of a singular C-point a line of circular polarization states is found. This line of circular polarizations in the focal plane represents a non-generic singularity (C-line in 2d space). Additionally, L-points are not generated either for this case since the zero-lines of 3(a2) $\gamma_{x,y,z}$ (red, yellow, green) have no joint intersection.

If we increase the topological charge l, C-points as well as L-points are created in the focal plane as evident from the intersections of the respective zero-lines. For 3(b) $l = 1$ and 3(c) $l = 2$ the polarization distribution includes 3(b1),(c1) six C-points and 3(b2),(c2) six L-points in regions where $|\boldsymbol{\mathcal{E}}|^2 \neq 0$. Furthermore, between two C-points there is always an L-point located and vice versa. The case with topological charge 3(d) $l = 3$ shows 3(d1) no C-point within the intensity structure $|\boldsymbol{\mathcal{E}}|^2 \neq 0$, but 3(d2) an individual L-point on the optical axis. In contrast, for 3(e) $l = 4$, 3(e2) no L-point is generated, but 3(e1) a C-point can be found on-axis. Here, two of each zero-lines of $\Re(\Psi_C)$ and $\Im(\Psi_C)$ intersect at the C-point marking a (non-generic) higher-order C-point or two very close generic C-points of first order. If the topological charge

Optics EXPRESS

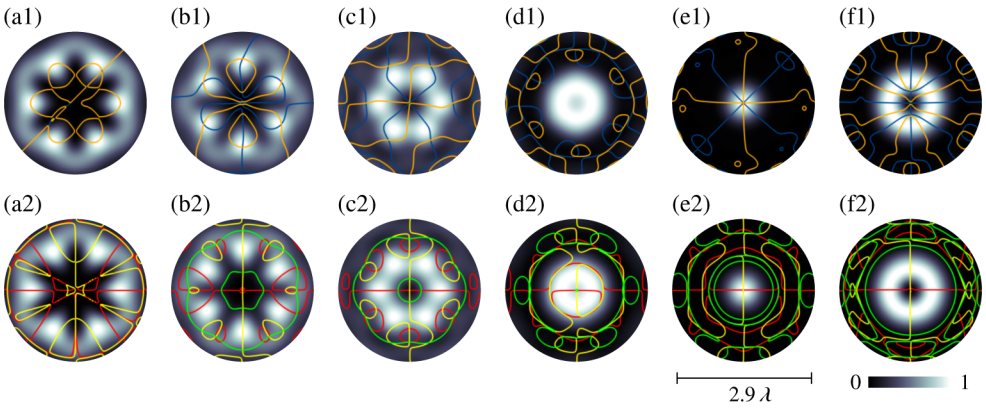

Fig. 3. Generic singularities in focal structures: We show the zero-lines inside the focal plane of a tightly focused higher-order vector beam with singularity index $\sigma_{12} = 8$ and additional topological charge $l \in [0, 5]$ in (a)-(f) with increasing l. The background shows the normalized intensity structure $|\mathcal{E}|^2 \in [0, 1]$. By examining the intersection points of the zero-lines, 1) C-points (blue, orange line: $\Re(\Psi_C) = 0$, $\Im(\Psi_C) = 0$) as well as 2) L-points (red, yellow, green line: $\gamma_{x,y,z} = 0$) can be detected. (color version online)

is increased to $l = 5$, 3(f1) two C-points and 3(f2) no L-point are created within the respective donut-like intensity structure.

In general, a defined relation between the focused higher-order vector beam with phase vortices and the generated polarization singularities can be observed. From the numerical simulations above and from additional calculations for vector beams with $\sigma_{12} \in [4, 12]$ and $l \in [0, 7]$ we derive

I)	$l = 0$	: no polarization singularity,
II)	$0 < l < \lvert\sigma_{12}\rvert/2 - 1$	: $\lvert\sigma_{12} - 2\rvert$C- and L-points,
III)	$l = \lvert\sigma_{12}/2 - 1\rvert$	: one L-point in the center,
IV)	$l = \lvert\sigma_{12}\rvert/2$	: one C-point in the center.

As evident from case II), the number of generated C- and L-points within the tight focus corresponds to the number of ζ-lines in the incident higher-order vector beam. Consequently, the ability to tailor the singularity index σ_{12} and the topological charge l of the incident vector beams in turn allows controlling the number of generated polarization singularities within the tight focus and, thus, to create complete polarization singularity networks [75] within the non-paraxial regime.

5. Creating an optical Möbius strip array

Polarization ellipses around generic polarization singularities may reveal intriguing 3d topological structures in non-paraxial light fields. Here, we restrict ourselves to topologies around C-points and investigate these by tracing the major axis of the polarization ellipses on a circle, which lies in the focal 2d plane around respective singularity.

In non-paraxial fields complex 3d topologies can be generated. In order to fully identify these topologies, we investigate three different projections onto different planes [40,71,72]. The first projection plane is the xy-plane, e.g. the focal plane, onto which the major axis is projected. For this projection plane, two indices I and Λ can be defined, where I describes the winding number of the projected axis for one cycle around the circle and Λ defines the number of ζ-lines created by the projections [43,44], respectively.

Optics EXPRESS

The two additional projection planes correspond to a radial plane τ_0 and a tangential plane π_0 [40,71,72] as visualized in Fig. 4. The major axis $\boldsymbol{\alpha}$ on the circle σ associated with different angles $\rho \in [0, 2\pi]$ is projected onto each plane τ_0 and π_0, resulting in the projections **R** and **T**, respectively. An index is referred to each projection plane, which defines the winding number of the major axis or the projections **R** and **T**, respectively, after a 2π-cycle around the circle σ. The indices can be calculated from [71,72]

$$\tau_\alpha = \frac{\delta(2\pi) - \delta(0)}{2\pi}, \qquad \pi_\alpha = \frac{\delta(2\pi) - \delta(0)}{2\pi}, \tag{5}$$

in which $\delta(\rho)$ corresponds to the angle between the projection **R** or **T** and the x'-axes.

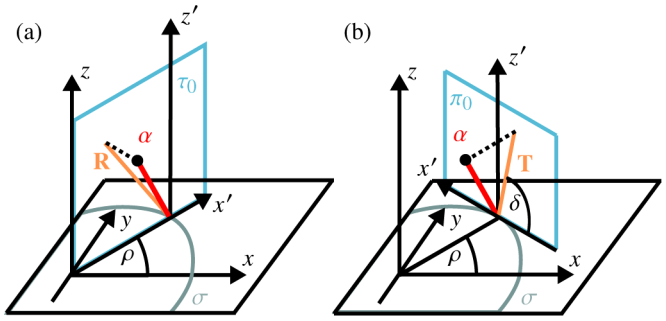

Fig. 4. Projection of the major axis $\boldsymbol{\alpha}$ of a polarization ellipse onto the (a) radial projection plane τ_0 and the (b) tangential projection plane π_0.

As an illustrative example, we explore a tightly focused vectorial flower structure with $\sigma_{12} = 8$ and an additional phase vortex of charge $l = 1$. In total, the focal structure contains six C-points (cf. Fig. 3(b1)). As shown in Fig. 5(a), we consider a circle (white dashed line) around the top C-point above the optical axis in a lobe of the intensity structure $|\mathcal{E}|^2$. Tracing the major axis $\boldsymbol{\alpha}$ of the polarization ellipses on this circle reveals a hidden optical polarization Möbius strip as visualized in Fig. 5(b). We observe the major axes (blue lines with blue and green endpoints) undergoing half a twist on circles surrounding this C-point. The projection of this Möbius strip onto the xy-plane shows a lemon-like [47] distribution in the polarization states' orientation with indices $I = 1$ and $\Lambda = 1$. The additional projection onto the radial and tangential plane τ_0 and π_0 are presented in Figs. 5(c) and 5(d), respectively, where solely the blue endpoints of the major axis are projected as red dots, while going along the circle. Both projections exhibit an index of $\tau_\alpha = \pi_\alpha = 1/2$. All indices and especially the identified Möbius strip topology is perfectly consistent with the theory presented in [71,72]. Note that, due to the complex surrounding polarization structure, we expect to observe multi-twist Möbius strips around a C-point of higher order (/ two very close first-order C-points) as tailored in Fig. 3(e1).

Up to this point, we analyzed the polarization topology around a single C-point and we deciphered an optical polarization Möbius strip. As presented above, the investigated focal structure does not only contain a single but six C-points. Hence, we expect complex polarization topologies around the other C-points as well, forming an intriguing 3d topology network. To investigate this, we extend our analysis and additionally explore the topologies around the other C-points. The results are presented in Fig. 5(e) revealing a unique optical polarization Möbius strip array in a tailored non-paraxial field which consists of six Möbius strips located around each C-point. To the best of our knowledge, such a complex structure has not yet been demonstrated. The major axes (blue lines with green and blue endpoints) and therefore the Möbius strips are depicted at the observed position within the normalized intensity structure $|\mathcal{E}(x, y, z = 0)|^2$. In the xy-plane the projections (blue lines) of each Möbius strip is shown. All Möbius strips entail

Optics EXPRESS

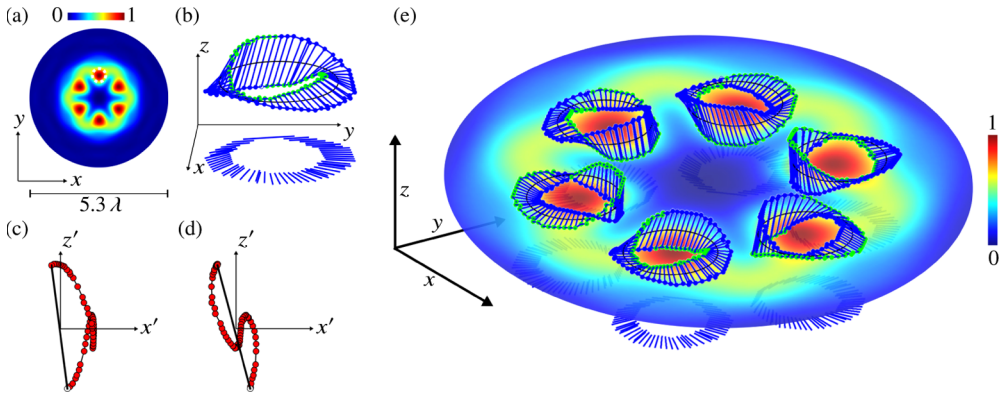

Fig. 5. Topologies around off-axis singularities: We explore a tightly focused vectorial flower with $\sigma_{12} = 8$ and phase vortex with $l = 1$, whose intensity structure $|\mathcal{E}|^2$ is shown in (a). Presented are the (b) 3d polarization topology around a C-point (white dashed line in (a)), which is formed by tracing the major axis, and the corresponding projections onto the planes (c) τ_0 and (d) π_0. Moreover, the overall polarization topology around all C-points is illustrated in (e), where the background corresponds to the total normalized intensity $|\mathcal{E}(x, y, 0)|^2$, revealing an optical polarization Möbius strip array.

the same structure with the same indices, whereby each Möbius stripe is oriented in such way that the ζ-lines point away from the optical axis. The number of created Möbius strips is equal to the number of C-points within the tight focus, which in turn can be controlled by tailoring the incident vectorial field. Consequently, by choosing a well-defined incident singularity index σ_{12} and a topological charge l, we are able to generate arbitrary optical Möbius strip arrays.

6. Conclusion

We demonstrated the customization of complex networks of generic 3d polarization singularities as well as intriguing 3d polarization topologies in non-paraxial structured 4d light fields. By tightly focusing tailored paraxial vector beams of chosen index σ_{12} combined with an additional phase vortex of charge l we realize focal light fields whose electric field components around the optical axis form cones and strips with a σ_{12}- and l-dependent number of twists. Beyond, we evince the control of generic L- and C-singularities, adapting their number and position by σ_{12} and l. These focal generic singularity networks embed interesting polarization topologies: each C-point corresponds to a half-twist Möbius strip, so that together they form a not yet observed optical Möbius strip array. Our results are forward-looking for the optical fabrication of novel functional media based on non-trivial topologies or the assembly of polarization sensitive particles via optical manipulation. For instance, polarization sensitive nano-objects could be arranged following custom polarization topologies in order to form novel functional chiral metasurfaces by bottom-up assembly. Beyond, our findings give new insights into the fundamentals of light, contributing to the investigation of 3d polarization structures including its complex singularities and topologies.

Funding

Deutsche Forschungsgemeinschaft (EXC 1003 – CiM, TRR61).

References

1. H. Rubinsztein-Dunlop, A. Forbes, M. V. Berry, M. R. Dennis, D. L. Andrews, M. Mansuripur, C. Denz, C. Alpmann, P. Banzer, T. Bauer, E. Karimi, L. Marrucci, M. Padgett, M. Ritsch-Marte, N. M. Litchinitser, N. P. Bigelow, C.

Optics EXPRESS

Rosales-Guzmán, A. Belmonte, J. P. Torres, T. W. Neely, M. Baker, R. Gordon, A. B. Stilgoe, J. Romero, A. G. White, R. Fickler, A. E. Willner, G. Xie, B. McMorran, and A. M. Weiner, "Roadmap on structured light," J. Opt. **19**(1), 013001 (2017).
2. M. S. Soskin and M. V. Vasnetsov, Singular Optics (Elsevier, 2001), vol. 42 of Progress in Optics, chap. 4, pp. 219–277.
3. M. R. Dennis, K. O'Holleran, and M. J. Padgett, Singular Optics: Optical Vortices and Polarization Singularities (Elsevier, 2009), vol. 53 of Progress in Optics, chap. 5, pp. 293–363.
4. D. L. Andrews, Structured light and its applications: An introduction to phase-structured beams and nanoscale optical forces (Academic Press, 2011).
5. H. He, M. E. J. Friese, N. R. Heckenberg, and H. Rubinsztein-Dunlop, "Direct observation of transfer of angular momentum to absorptive particles from a laser beam with a phase singularity," Phys. Rev. Lett. **75**(5), 826–829 (1995).
6. M. Padgett and R. Bowman, "Tweezers with a twist," Nat. Photonics **5**(6), 343–348 (2011).
7. M. Woerdemann, C. Alpmann, M. Esseling, and C. Denz, "Advanced optical trapping by complex beam shaping," Laser Photonics Rev. **7**(6), 839–854 (2013).
8. G. Gibson, J. Courtial, M. Padgett, M. Vasnetsov, V. Pas'ko, S. Barnett, and S. Franke-Arnold, "Free-space information transfer using light beams carrying orbital angular momentum," Opt. Express **12**(22), 5448–5456 (2004).
9. A. Mair, A. Vaziri, G. Weihs, and A. Zellinger, "Entanglement of the orbital angular momentum states of photons," Nature **412**(6844), 313–316 (2001).
10. M. Mirhosseini, O. S. Maga na-Loaiza, M. N. O'Sullivan, B. Rodenburg, M. Malik, M. P. Lavery, M. J. Padgett, D. J. Gauthier, and R. W. Boyd, "High-dimensional quantum cryptography with twisted light," New J. Phys. **17**(3), 033033 (2015).
11. B. Ndagano, B. Perez-Garcia, F. S. Roux, M. McLaren, C. Rosales-Guzmán, Y. Zhang, O. Mouane, R. I. Hernandez-Aranda, T. Konrad, and A. Forbes, "Characterizing quantum channels with non-separable states of classical light," Nat. Phys. **13**(4), 397–402 (2017).
12. M. Meier, V. Romano, and T. Feurer, "Material processing with pulsed radially and azimuthally polarized laser radiation," Appl. Phys. A **86**(3), 329–334 (2007).
13. J. J. Nivas, F. Cardano, Z. Song, A. Rubano, R. Fittipaldi, A. Vecchione, D. Paparo, L. Marrucci, R. Bruzzese, and S. Amoruso, "Surface structuring with polarization-singular femtosecond laser beams generated by a q-plate," Sci. Rep. **7**(1), 42142 (2017).
14. A. Belmonte and J. P. Torres, "Optical doppler shift with structured light," Opt. Lett. **36**(22), 4437–4439 (2011).
15. C. Rosales-Guzmán, N. Hermosa, A. Belmonte, and J. P. Torres, "Experimental detection of transverse particle movement with structured light," Sci. Rep. **3**(1), 2815 (2013).
16. S. W. Hell and J. Wichmann, "Breaking the diffraction resolution limit by stimulated emission: stimulated-emission-depletion fluorescence microscopy," Opt. Lett. **19**(11), 780–782 (1994).
17. D. P. Biss, K. S. Youngworth, and T. G. Brown, "Dark-field imaging with cylindrical-vector beams," Appl. Opt. **45**(3), 470–479 (2006).
18. J. A. Davis, D. M. Cottrell, J. Campos, M. J. Yzuel, and I. Moreno, "Encoding amplitude information onto phase-only filters," Appl. Opt. **38**(23), 5004–5013 (1999).
19. C. Maurer, A. Jesacher, S. Fürhapter, S. Bernet, and M. Ritsch-Marte, "Tailoring of arbitrary optical vector beams," New J. Phys. **9**(3), 78 (2007).
20. W. Han, Y. Yang, W. Cheng, and Q. Zhan, "Vectorial optical field generator for the creation of arbitrarily complex fields," Opt. Express **21**(18), 20692–20706 (2013).
21. Z. Chen, T. Zeng, B. Qian, and J. Ding, "Complete shaping of optical vector beams," Opt. Express **23**(14), 17701–17710 (2015).
22. E. Otte, C. Schlickriede, C. Alpmann, and C. Denz, "Complex light fields enter a new dimension: holographic modulation of polarization in addition to amplitude and phase," Proc. SPIE **9379**, 937908 (2015).
23. C. Alpmann, C. Schlickriede, E. Otte, and C. Denz, "Dynamic modulation of Poincaré beams," Sci. Rep. **7**(1), 8076 (2017).
24. L. Marrucci, C. Manzo, and D. Paparo, "Optical spin-to-orbital angular momentum conversion in inhomogeneous anisotropic media," Phys. Rev. Lett. **96**(16), 163905 (2006).
25. E. J. Galvez and S. Khadka, "Poincaré modes of light," Proc. SPIE **8274**, 82740Y (2012).
26. C. Rosales-Guzmán, N. Bhebhe, and A. Forbes, "Simultaneous generation of multiple vector beams on a single SLM," Opt. Express **25**(21), 25697–25706 (2017).
27. E. Otte, C. Rosales-Guzmán, B. Ndagano, C. Denz, and A. Forbes, "Entanglement beating in free space through spin-orbit coupling," Light: Sci. Appl. **7**(5), 18009 (2018).
28. Y.-Y. Xie, Z.-J. Cheng, X. Liu, B.-Y. Wang, Q.-Y. Yue, and C.-S. Guo, "Simple method for generation of vector beams using a small-angle birefringent beam splitter," Opt. Lett. **40**(21), 5109–5112 (2015).
29. M. V. Berry, M. R. Dennis, and R. L. Lee Jr, "Polarization singularities in the clear sky," New J. Phys. **6**, 162 (2004).
30. E. Otte, K. Tekce, and C. Denz, "Spatial multiplexing for tailored fully-structured light," J. Opt. **20**(10), 105606 (2018).

Optics EXPRESS

31. E. Otte, K. Tekce, S. Lamping, B. J. Ravoo, and C. Denz, "Polarization nano-tomography of tightly focused light lansdscapes by self-assembled monolayers," *In formal peer review process Nat. Commun.* NCOMMS-19-00484B, (2019).
32. S. Quabis, R. Dorn, M. Eberler, O. Glöckl, and G. Leuchs, "Focusing light to a tighter spot," Opt. Commun. **179**(1-6), 1–7 (2000).
33. R. Dorn, S. Quabis, and G. Leuchs, "Sharper focus for a radially polarized light beam," Phys. Rev. Lett. **91**(23), 233901 (2003).
34. E. Otte, K. Tekce, and C. Denz, "Tailored intensity landscapes by tight focusing of singular vector beams," Opt. Express **25**(17), 20194–20201 (2017).
35. Q. Zhan, "Cylindrical vector beams: from mathematical concepts to applications," Adv. Opt. Photonics **1**(1), 1–57 (2009).
36. W. Chen and Q. Zhan, "Three-dimensional focus shaping with cylindrical vector beams," Opt. Commun. **265**(2), 411–417 (2006).
37. N. Bokor and N. Davidson, "Generation of a hollow dark spherical spot by 4pi focusing of a radially polarized Laguerre-Gaussian beam," Opt. Lett. **31**(2), 149–151 (2006).
38. H. Wang, L. Shi, B. Lukyanchuk, C. Sheppard, and C. T. Chong, "Creation of a needle of longitudinally polarized light in vacuum using binary optics," Nat. Photonics **2**(8), 501–505 (2008).
39. F. Qin, K. Huang, J. Wu, J. Jiao, X. Luo, C. Qiu, and M. Hong, "Shaping a subwavelength needle with ultra-long focal length by focusing azimuthally polarized light," Sci. Rep. **5**(1), 9977 (2015).
40. I. Freund, "Cones, spirals, and Möbius strips, in elliptically polarized light," Opt. Commun. **249**(1-3), 7–22 (2005).
41. T. Bauer, P. Banzer, E. Karimi, S. Orlov, A. Rubano, L. Marrucci, E. Santamato, R. W. Boyd, and G. Leuchs, "Observation of optical polarization Möbius strips," Science **347**(6225), 964–966 (2015).
42. T. Bauer, M. Neugebauer, G. Leuchs, and P. Banzer, "Optical polarization Möbius strips and points of purely transverse spin density," Phys. Rev. Lett. **117**(1), 013601 (2016).
43. J. F. Nye, Natural focusing and fine structure of light: caustics and wave dislocations (CRC Press, 1999).
44. J. F. Nye, "Monstars on glaciers," J. Glaciol. **29**(101), 70–77 (1983).
45. J. F. Nye, "Lines of circular polarization in electromagnetic wave fields," Proc. R. Soc. London, Ser. A **389**(1797), 279–290 (1983).
46. J. F. Nye and J. V. Hajnal, "The wave structure of monochromatic electromagnetic radiation," Proc. R. Soc. London, Ser. A **409**(1836), 21–36 (1987).
47. E. J. Galvez, Light Beams with Spatially Variable Polarization (John Wiley & Sons, 2015), vol. 1 of Photonics – Fundamentals of Photonics and Physics, chap. 3, pp. 61–76.
48. E. J. Galvez, I. Dutta, K. Beach, J. J. Zeosky, J. A. Jones, and B. Khajavi, "Multitwist Möbius strips and twisted ribbons in the polarization of paraxial light beams," Sci. Rep. **7**(1), 13653 (2017).
49. C. Wan and Q. Zhan, "Generation of exotic optical polarization Möbius strips," Opt. Express **27**(8), 11516–11524 (2019).
50. A. Garcia-Etxarri, "Optical polarization Möbius strips on all-dielectric optical scatterers," ACS Photonics **4**(5), 1159–1164 (2017).
51. T. Bauer, P. Banzer, F. Bouchard, S. Orlov, L. Marrucci, E. Santamato, R. W. Boyd, E. Karimi, and G. Leuchs, "Multi-twist polarization ribbon topologies in highly-confined optical fields," New J. Phys. **21**(5), 053020 (2019).
52. P. Huo, S. Zhang, Q. Fan, Y. Lu, and T. Xu, "Photonic spin-controlled generation and transformation of 3D optical polarization topologies enabled by all-dielectric metasurfaces," Nanoscale **11**(22), 10646–10654 (2019).
53. E. Otte, C. Alpmann, and C. Denz, "Higher-order polarization singularitites in tailored vector beams," J. Opt. **18**(7), 074012 (2016).
54. Q. Zhan, Vector beams (CRC Press, 2014), chap. 9, pp. 239–271, Laser beam propagation: generation and propagation of customized light.
55. D. G. Hall, "Vector-beam solutions of Maxwell's wave equation," Opt. Lett. **21**(1), 9–11 (1996).
56. E. J. Galvez, Vector beams in free space (Cambridge University Press, 2013), chap. 3, pp. 51–70, The angular momentum of light.
57. I. Freund, "Polarization singularity indices in Gaussian laser beams," Opt. Commun. **201**(4-6), 251–270 (2002).
58. I. Freund, "Polarization flowers," Opt. Commun. **199**(1-4), 47–63 (2001).
59. E. Otte, C. Alpmann, and C. Denz, "Polarization singularity explosions in tailored light fields," Laser Photonics Rev. **12**(6), 1700200 (2018).
60. B. Richards and E. Wolf, Electromagnetic diffraction in optical systems. II. Structure of the image field in an aplanatic system, in *Proceedings of the Royal Society of London A: Mathematical, Physical and Engineering Sciences*, vol. 253 (The Royal Society, 1959), pp. 358–379.
61. K. Youngworth and T. Brown, "Focusing of high numerical aperture cylindrical-vector beams," Opt. Express **7**(2), 77–87 (2000).
62. B. Boruah and M. Neil, "Focal field computation of an arbitrarily polarized beam using fast fourier transforms," Opt. Commun. **282**(24), 4660–4667 (2009).
63. R. W. Schoonover and T. D. Visser, "Polarization singularities of focused, radially polarized fields," Opt. Express **14**(12), 5733–5745 (2006).

Optics EXPRESS

64. W. Zhang, S. Liu, P. Li, X. Jiao, and J. Zhao, "Controlling the polarization singularities of the focused azimuthally polarized beams," Opt. Express **21**(1), 974–983 (2013).
65. M. Berry and M. Dennis, "Polarization singularities in isotropic random vector waves," Proc. R. Soc. London, Ser. A **457**(2005), 141–155 (2001).
66. M. R. Dennis, "Fermionic out-of-plane structure of polarization singularities," Opt. Lett. **36**(19), 3765–3767 (2011).
67. C. J. R. Sheppard, "Jones and Stokes parameters for polarization in three dimensions," Phys. Rev. A **90**(2), 023809 (2014).
68. T. Setälä, A. Shevchenko, M. Kaivola, and A. T. Friberg, "Degree of polarization for optical near fields," Phys. Rev. E **66**(1), 016615 (2002).
69. M. V. Berry, "Index formulae for singular lines of polarization," J. Opt. A: Pure Appl. Opt. **6**(7), 675–678 (2004).
70. E. Otte, K. Tekce, and C. Denz, "Customized focal light landscapes by complex vectorial fields for advanced optical trapping," Proc. SPIE **10549**, 105490S (2018).
71. I. Freund, "Optical Möbius strips in three-dimensional ellipse fields: I. Lines of circular polarization," Opt. Commun. **283**(1), 1–15 (2010).
72. I. Freund, "Optical Möbius strips in three dimensional ellipse fields: II. Lines of linear polarization," Opt. Commun. **283**(1), 16–28 (2010).
73. M. R. Dennis, "Topological singularities in wave fields," Ph.D. thesis, University of Bristol, (2001).
74. M. S. Soskin and M. V. Vasnetsov, Second international conference on singular optics (optical vortices): Fundamentals and applications, in *Second International Conference on Singular Optics (Optical Vortices): Fundamentals and Applications*, vol. 4403, (2001).
75. E. Otte and C. Denz, "Sculpting complex polarization singularity networks," Opt. Lett. **43**(23), 5821–5824 (2018).